Swift unveils the orbital period of IGR J18214-1318

G. Cusumano [ID],★ A. D'Aì [ID], A. Segreto, V. La Parola and M. Del Santo
INAF, Istituto di Astrofisica Spaziale e Fisica Cosmica, Via U. Malfa 153, I-90146 Palermo, Italy

ABSTRACT

We analysed 13 yr of the Neil Gehrels Swift Observatory survey data collected on the high-mass X-ray binary IGR J18214-1318. Performing the timing analysis, we detected a periodic signal of 5.42 d. From the companion star characteristics, we derived an average orbital separation of $\sim 41 R_\odot \simeq 2 R_\star$. The spectral type of the companion star (O9) and the tight orbital separation suggest that IGR J18214-1318 is a wind-accreting source with eccentricity lower than 0.17. The intensity profile folded at the orbital period shows a deep minimum compatible with an eclipse of the source by the companion star. In addition, we report on the broad-band 0.6–100 keV spectrum using data from *XMM–Newton*, *NuSTAR*, and *Swift*, applying self-consistent physical models. We find that the spectrum is well fitted either by a pure thermal Comptonization component, or, assuming that the source is a neutron star accreting above the critical regime, by a combined thermal and bulk motion Comptonization model. In both cases, the presence of a local neutral absorption (possibly related to the thick wind of the companion star) is required.

Key words: X-rays: binaries – X-rays: individual: IGR J18214-1318.

1 INTRODUCTION

During the last two decades, astronomers have taken advantage of two prolific telescopes in the hard X-ray domain: the IBIS/ISGRI telescope (Lebrun et al. 2003; Ubertini et al. 2003) on board the *International Gamma-Ray Astrophysics Laboratory* (*INTEGRAL*) satellite (Winkler et al. 2003) and the Burst Alert Telescope (BAT; Barthelmy et al. 2005) on board the *Neil Gehrels Swift Observatory* (Gehrels et al. 2004; hereafter *Swift*). IBIS/ISGRI has performed a deep and continuous scanning of the Galactic plane along the years revealing a large number of new X-ray sources, among which many were high-mass X-ray binaries (HMXBs). These are usually distinguished into two sub-groups based on the observed spectral emission and variability: obscured HMXBs and supergiant fast X-ray transients (in't Zand 2005; Sguera et al. 2005; Negueruela et al. 2006; Bozzo et al. 2017; Martinez-Nunez et al. 2017). The former are immersed in the wind from the companion star and, as a consequence, strong absorption have made their detection harder for soft X-ray instruments; the latter group shows very bright, but rapidly transient flares, and were revealed because of the continuous scan of the Galactic plane performed by *INTEGRAL*. The association of these sources to the class of HMXBs has been inferred either through the discovery of their optical counterparts (e.g. Filliatre & Chaty 2004; Reig et al. 2005; Masetti et al. 2006; Negueruela et al. 2006; Zurita Heras & Chaty 2008) or by the observation of long periodicities. These can be due either to the occultation of the neutron star (NS) by the supergiant companion or to the periodic enhancement of their X-ray emission at the periastron passage of the NS in an eccentric orbit. BAT is playing an important role in the study of many of these new *INTEGRAL* sources. Because of its large field of view (1.4 steradians half coded) and to frequent changes in the satellite pointing direction,

BAT monitors daily ~ 90 per cent of the sky, making it an efficient tool to detect transient phenomena from known and unknown sources (Krimm et al. 2013). Combining the entire time span of its survey data, several long periodicities of HMXBs have been revealed (e.g. Corbet & Krimm 2009; Corbet, Krimm & Skinner 2010a; Corbet et al. 2010b,c,d; Corbet & Krimm 2010; Cusumano et al. 2010; La Parola et al. 2010; D'Aì et al. 2011a,b; Cusumano et al. 2013a,b; La Parola et al. 2013; Segreto et al. 2013a,b; La Parola et al. 2014; D'Aì et al. 2015; Cusumano et al. 2015, 2016).

In this work, we present a temporal and spectral analysis of IGR J18214-1318, a source discovered by *INTEGRAL* on the Galactic plane. This source was observed with a flux of ~ 1m Crab in the energy band 17–60 keV (Bird et al. 2006; Krivonos et al. 2012; Bird et al. 2016) and localized through a *Chandra* observation at coordinates (J2000) RA = 18h21m19.76s, Dec. $= -13°18'38''.9$ (Tomsick et al. 2008). IGR J18214-1318 is associated to USNO-B1.0 0766-0475700, most likely a O9I star, and classified as an obscured HMXB (Butler et al. 2009). The *Chandra* spectrum is well modelled by a simple power law with a photon index $\Gamma = 0.7^{+0.6}_{-0.5}$, absorbed by an equivalent absorption column $N_{\rm H} = (1.2 \pm 0.3) \times 10^{23}$ cm^{-2}. Using *Swift* data, Rodriguez, Tomsick & Chaty (2009) measured a photon index of $\Gamma = 0.4 \pm 0.2$ and a column density of $N_{\rm H} = 3.5^{+0.8}_{-0.5} \times 10^{22}$ cm^{-2}, significantly lower than the value measured with *Chandra* and consistent with the Galactic $N_{\rm H}$ along the line of sight to IGR J18214-1318. A high-statistics broad-band spectrum from data collected by *XMM–Newton* (Jansen et al. 2001) and *NuSTAR* (Harrison et al. 2013) could be well modelled in the hard X-ray region with a power law modified by an exponential cut-off with e-folding energy <25 keV and a cut-off at ~ 10 keV. In the softer band, an equivalent fit could be obtained either by adding a blackbody component with a temperature of ~ 1.74 keV or with a partial covering absorber of $\sim 10^{23}$ cm^{-2} and ~ 77 per cent of covering fraction (Fornasini et al. 2017). In both cases, an iron Kα emission line at 6.4 keV was detected with an equivalent width ~ 55 eV. Timing analysis did not reveal any

★ E-mail: cusumano@ifc.inaf.it

Table 1. Observations log. The quoted orbital phase refers to the profile reported in the middle panel of Fig. 1.

Obs #	Observatory	Instrument	Obs ID	T_{start} MJD	Exposure (ks)	Rate (c/s)	Orb. Phase
1	*Swift*	XRT	00035354001	53777.646	6.3	0.30 ± 0.01	0.44
2	*Swift*	XRT	00035354003	56240.844	0.7	0.15 ± 0.01	0.52
3	*Swift*	XRT	00035354005	57702.037	0.5	...	0.89
4	*Swift*	XRT	00035354006	58064.671	0.8	0022 ± 0.005	0.74
5	*NuSTAR*	FPMA	3000114002	56918.107	26.3	0.56 ± 0.01	0.37
		FPMB	–	–	26.3	0.55 ± 0.01	–
6	*XMM–Newton*	EPIC–pn	0741470201	56918.053	18.6	1.19 ± 0.01	0.36
		EPIC–MOS1	–	–	25.9	0.37 ± 0.004	–
		EPIC–MOS2	–	–	25.9	0.37 ± 0.004	–

Table 2. Best-fitting spectral parameters for the two models discussed in the paper.

Parameter	Units	Values	
		nthcomp	bwcycl
$N_{H,\ gal}$	10^{22} cm^{-2}	1.3	1.3
$N_{H,\ pc}$	10^{22} cm^{-2}	4.3 ± 0.4	$9.6^{1.7}_{-0.8}$
$F^a_{n_H,part}$	–	0.89 ± 0.02	$0.76^{0.04}_{-0.08}$
Γ	–	2.07 ± 0.03	–
kT_{bb}	keV	1.39 ± 0.04	–
kT_e	keV	20 (fixed)	–
ξ	–	–	2.07 ± 0.17
δ	–	–	$6.2^{3.0}_{-1.4}$
T_e	keV	–	$4.8^{0.1}_{-0.2}$
R_o	m	–	5.5 ± 0.3
Flux^b	–	6.0	6.1
C^c_{FPMB}	–	1.04 ± 0.02	1.04 ± 0.02
C^c_{PN}	–	0.80 ± 0.01	0.80 ± 0.01
$C^c_{MOS1/MOS2}$	–	0.84 ± 0.02	0.84 ± 0.02
χ^2 / (d.o.f.)	–	421/418	425/418

^{a}Covering fraction for n_H, *part*. ^{b}We report the unabsorbed (both for the Galactic and the local components) bolometric fluxes in the 0.1–100 keV with respect to the *NuSTAR*/FPMA data set in units of 10^{-11} erg cm^{-2} s^{-1}. ^{c}Multiplicative factors of the model for each data set. We used the reference constant of 1 for the *Nu*STARFPMA data set.

periodicity in the frequency range 0.1–88 Hz with a 90 per cent upper limit on the rms noise level of 2.2 per cent.

This paper is organized as follows: Section 2 describes the data reduction and the calibration procedures applied to the data; in Sections 3 and 4 we describe our timing and spectral analysis; in Section 5 we discuss our results.

2 DATA REDUCTION

We used data or thi work from BAT, XRT (X-ray Telescope Burrows et al. 2004), *XMM–Newton*, and *NuSTAR*.

We retrieved BAT survey data between 2004 December and 2017 February from the HEASARC public archive[1] and processed them using the BATIMAGER code (Segreto et al. 2010), dedicated to the processing of coded mask instrument data. IGR J18214-1318 is detected with a significance of 24.7 standard deviations in the 20–85 keV all-

sky map. For the timing analysis, we extracted a light curve in the same energy range with the maximum available time resolution of ~ 300 s and corrected to the solar system barycentre using the task EARTH2SUN[2] and the JPL DE-200 ephemeris (Standish 1982). For the spectral analysis, we produced the background-subtracted spectrum in eight energy channels, averaged over the entire exposure, and we used the official BAT spectral redistribution matrix.[3]

XRT observed IGR J18214-1318 four times. The source was always observed in Photon Counting (PC) mode (Hill et al. 2004) for a total exposure of ~ 9.4 ks. The details on the XRT observations are reported in Table 1. We processed the data using standard filtering and screening criteria (0–12 grade selection, XRTPIPELINE, v.0.12.4). IGR J18214-1318 was detected in three observations. The source events were extracted from a circular region (20 pixel radius, with 1 pixel = 2.36 arcsec) centred on the source coordinates (Tomsick et al. 2008). The background for the spectral analysis was extracted from an annular region with inner and outer radii 30 and 70 pixels, respectively. XRT ancillary response file were generated with XRTMKARF[4]; we used the spectral redistribution matrix v014. For the spectral analysis, we used only events from Obs.ID 00035354001 because of its much higher signal-to-noise ratio with respect to the other observations. XRT energy channels were binned requiring a minimum of 20 counts per bin in order to use the χ^2 statistics.

NuSTAR and *XMM–Newton* observed IGR J18214-1318 simultaneously on 2014 September 18. Details of these two observations are reported in Fornasini et al. (2017) and summarized in Table 1. We re-extracted data for spectral analysis using NUSTARDAS v1.5.1 and the SAS v15.5.0 for *Nu*STAR and XMM–*Newton*, respectively. We applied standard selection criteria and source and background regions. Spectral analysis was performed using XSPEC v.12.5. and spectral errors are given at 90 per cent confidence level.

3 TIMING ANALYSIS

We searched for periodicities in the 1–1000 d range in the BAT survey data using the folding technique and selecting events in the 20–85 keV energy range for optimal SNR. The time resolution is given by $\Delta P = P^2/(N\,\Delta T)$, where P is the trial period, $N = 16$ is the number of phase bins used to build the trial profile, and $\Delta T =404.4$ Ms is the data time span. The BAT survey data present a large spread of statistical errors mainly due to the wide range of off-axis directions in which the source is observed. To overcome this issue, the rate in the folded
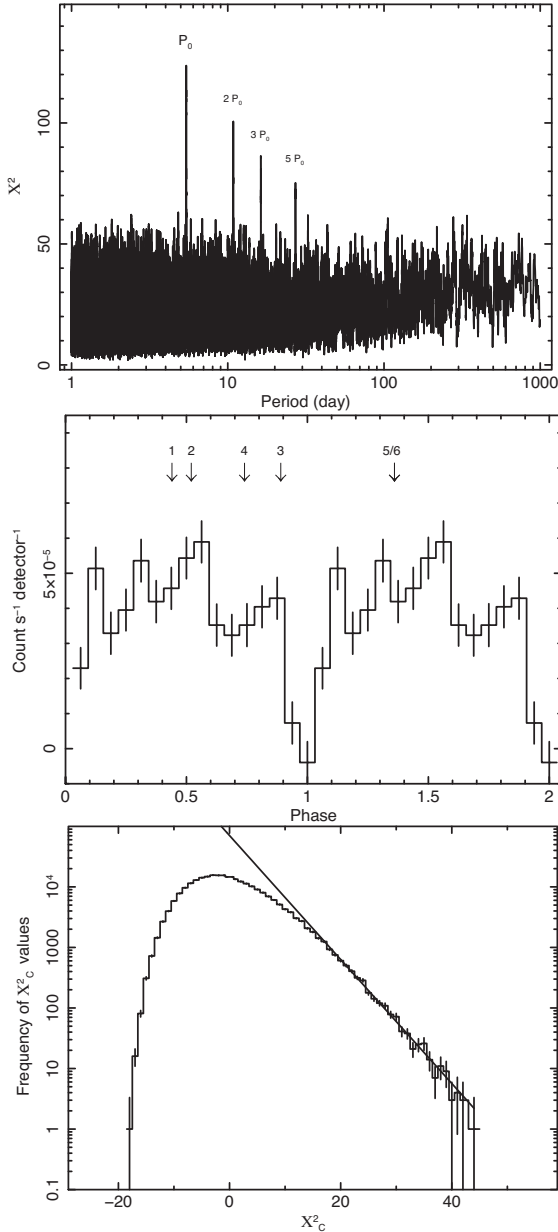
Figure 1. Top panel: Periodogram of BAT (20–85 keV) data for IGR J18214-1318. Middle panel: Light curve folded at a period $P_0 = 5.4246$ d, with 16 phase bins. The arrows mark the orbital phase of the XRT observations (1–4) and of the *XMM–Newton*, *NuSTAR* observations (5/6). Bottom panel: Histogram distribution of the χ_c^2 values; the solid line is the exponential function that best fits the right tail of the distribution.

profile for each trial period was weighted by the inverse square of the corresponding statistical error (see Cusumano et al. 2010). The resulting periodogram (top panel in Fig. 1) shows several features emerging above the noise: the highest peak is at $P_0 = 5.4246 \pm 0.0004$ d ($\chi^2 \sim 123$; the error is the period resolution at P_0). The other peaks are multiples of P_0 (two, three, and five times P_0). The intensity profile (middle panel in Fig. 1) at P_0 with $T_{epoch} = 55684.71093750$ MJD shows a flat intensity level and a deep minimum with intensity consistent with no emission. The centroid of the minimum, evaluated by fitting the data around the dip with a Gaussian model, is at a phase 0.987 ± 0.010 corresponding to $T_{min} = (55684.64 \pm 0.05) \pm nP_0$ MJD.

The time variability of the source causes the average χ^2 in the periodogram to significantly deviates from the average value expected for white noise (N–1). As a consequence, the χ^2 statistics cannot be applied to evaluate the significance of the detected periodicity. Therefore, we determined the significance of the feature from the data in the periodogram adopting the following methodology:

(i) We fit the periodogram with a second-order polynomial; a new χ_c^2 periodogram was obtained by subtracting the best-fitting trend from the original χ^2 distribution. In the new periodogram the P_0 ha a χ_c^2 value of 102.8.

(ii) We build the histogram of the χ_c^2 distribution (Fig. 1 bottom) selecting the values in the period interval between 1 and 10 d, excluding the values within an interval centred on P_0 and $10 \times \Delta P_0$ wide.

(iii) The tail ($\chi_c^2 > 20$) of the histogram is fitted with an exponential function and its integral between 102.8 and infinity, normalized for the total area below the histogram, is evaluated.

The value we obtain (3.3×10^{-11}) represents the probability of random occurrence for $\chi_c^2 > 102.8$ and corresponds to a significance of 6.6 standard deviations in Gaussian statistics.

The rate observed in the XRT observations (Table 1 and middle panel in Fig. 1) shows a strong variability that cannot be explained with the shape of the BAT folded profile. Observation 3, where the source is not detected, is close to the dip of the pulse profile, while observation 4, that shows a rate ~ 10 times lower than observations 1 and 2, is far from the dip.

4 SPECTRAL ANALYSIS

We re-analysed the data from simultaneous *NuSTAR* and *XMM–Newton* observations performed in 2014, previously reported in Fornasini et al. (2017). We aim at giving additional information on the the source using physical models to explain the broad-band X-ray emission. As a first check, we re-extracted the data and re-binned each spectrum according to the prescriptions outlined in Kaastra & Bleeker (2016).[5] We applied the same models used by Fornasini et al. (2017) and obtained, within the statistical uncertainties, consistent parameters values. Fornasini et al. (2017) showed that the spectrum is well fitted by a phenomenological model composed of a power law with a high-energy cut-off; in addition, in the softer band, the spectrum needs either a soft blackbody or a partial covering component, which were found statistically equivalent. It is known that the exponentially high-energy cut-off is an empirical model that suffers from artefacts due to the discontinuity created by the model at the cut-off energy. As discussed in Fornasini et al. (2017), the spectral shape of IGR J18214-1318 is compatible with the emission observed in accreting X-ray pulsars, even though a search for coherent pulsations did not reveal any periodic signal. In this scenario, the high-energy X-ray emission is dominated by the emission from the shock in the accreting column. The free-falling plasma is slowed down within few free path lengths by the presence of Coulomb, or radiative, shock depending on the pulsar being in the critical regime, or not (Becker & Wolff 2005, 2007). In both cases, most of the hard X-ray radiation escapes either by bulk-motion or thermal Comptonization processes in the post-shock region. At high accretion rates, thermal Comptonization should be the dominant channel and pulsar spectra clearly show a cut-off at the

---

[5]We used the ad hoc script written by C. Ferrigno at https://gitlab.astro.unige.ch/ferrigno/optimal-binning.

electron thermal temperature superimposed on the hard power-law emission ($\Gamma < 2$). At lower accretion rates, spectra appear softer and with higher, or absent, roll-over. We first adopted a model of pure thermal Comptonization and then applied a self-consistent X-ray pulsar model, where all the main physical mechanisms are taken into account (model `bwcycl` Becker & Wolff 2005, 2007; Ferrigno et al. 2009) and then compared the results.

To model the thermal Comptonization, we adopted the `nthcomp` model in XSPEC (Zdziarski, Johnson & Magdziarz 1996; Zycki, Done & Smith 1999). The soft seed photons with a blackbody spectrum of temperature kT_{bb}, produced in the NS polar cap or in the post-shock region, are upscattered by an electron population at temperature kT_e that is related to the spectral high-energy cut-off. The model includes a fixed zero-width 6.4 keV line to fit the Fe Kα emission and multiplicative factors for each data set to account for slight differences in the instrument intercalibration (we fixed to 1 the FPMA constant, and set the EPIC/MOS1 and EPIC/MOS2 to be the same). Line-of-sight interstellar absorption is modelled using the `tbabs` component, using cross-sections from Verner et al. (1996) and element abundances from Wilms, Allen & McCray (2000). As in Fornasini et al. (2017), we also found that residuals were present below 2 keV and the final fit result was not satisfactory (χ^2/d.o.f. = 465/428). Analogously, we added to this continuum model a blackbody component, or, alternatively, a partial covering component. In the first scenario, we found a blackbody temperature of 1.5 ± 0.1 keV and a corresponding blackbody radius of 0.4 ± 0.1 km; the interstellar absorption column, $N_{H, gal}$, was left free to vary and the best-fit value was $(3.90 \pm 0.15) \times 10^{22}$ cm^{-2} These values are compatible with the corresponding estimates reported in Fornasini et al. (2017). In the second scenario, we fixed the interstellar absorption to the Galactic expected value[6] of 1.3×10^{22} cm^{-2} (HI4PI Collaboration 2016) and found an excess of local absorption of $(4.3 \pm 0.4) \times 10^{22}$ cm^{-2} and an absorbed fraction of 89 ± 2 per cent. However, unlike in Fornasini et al. (2017), the partial covering model gave us a significantly better χ^2 value (χ^2/d.o.f. = 421/415) than that obtained by adding the blackbody component (χ^2/d.o.f. = 455/415). This statistical difference is mainly ascribed to the different spectral binning, because we noted a similar statistical difference for these two scenarios also adopting the phenomenological continuum adopted in Fornasini et al. (2017).

It is worth noticing here that the fit sets only a poor constraint to the electron temperature, with a lower limit of 13 keV (95 per cent confidence interval). Thus, we chose to fix it to a reference value of 20 keV since this is a typical value found in other accreting X-ray pulsars at similar luminosity (Coburn et al. 2002). As a second step, we used the `bwcycl` model, assuming that the compact object is an accreting NS. This model has many parameters, most of which are strongly correlated, and it is important to fix as many of them as possible. In our context, we set to the default values the mass and the radius of the NS ($R_{NS} = 10$ km, $M_{NS} = 1.4 M_\odot$), we assumed a distance of 10 kpc, an NS magnetic field of 4×10^{12} G. From the `nthcomp` model, we derived a bolometric luminosity of $\sim 10^{36}$ erg s^{-1}, so we set for this model a mass accretion rate of 10^{16} g s^{-1}. We left free to vary the following parameters: ξ, related to the escaping time of photons, δ, related to the ratio of the bulk versus the thermal contribution of the whole Comptonized component, r_0, the radius of the accretion column and T_e, the temperature of the hot electrons (see Becker & Wolff 2007, for an extended discussion

on the physical meaning of these parameters). This model gave a poor statistical fit to the data (χ^2/d.o.f. = 659/428), leaving a pattern of residuals reminiscent of the one obtained applying only the thermal Comptonization model. Again, we looked for the best-fitting model adding either a blackbody or a partial covering model, and, similar to what obtained with the `nthcomp` model, we found a better description using the partial covering scenario (the χ^2/d.o.f. is 506/415 and 425/415, for the blackbody and partial covering scenarios, respectively). Since for both physical models we got better statistical results using a partial covering, and following Fornasini et al. (2017) who discussed the weakness of the blackbody interpretation, hereafter we shall focus only on the partial covering scenario. We show in Fig. 2 the data, the best-fitting models and residuals for the two models, and report in Table 2 the best-fitting parameter values and errors. For both models, the iron line is well described by the same set of values: the energy is 6.39 ± 0.03 keV, the line width is determined only as an upper limit of 85 eV (at 95 per cent confidence level); after freezing the width to zero, we derived a line normalization of $(1.7 \pm 0.4) \times 10^{-5}$ photons cm^{-2} s^{-1} and a corresponding equivalent width of 54 ± 2 eV.

Finally, we also analysed the *Swift* data, using the XRT data from ObsID 00035354001, for which there is the highest statistics, and the time-averaged BAT spectrum. The 1–10 keV X-ray spectrum is variable because of the changing of the local conditions on the neutral absorption and of the accretion rate, while the hard X-ray spectrum, above 15 keV, is generally dominated by the exponential tail of the Comptonized component, and depends only on the electrons temperature and the instantaneous mass accretion rate. Assuming there is no significant change in the electrons temperature, we left a multiplicative constant free to vary to keep into account the intercalibration between the two instruments and the different flux level. We find that an absorbed thermal Comptonization gives a good description of the data (χ^2/d.o.f. = 48/60), though spectral parameters are not so well constrained as in the previous case. We fixed the expected interstellar equivalent hydrogen column to 1.3×10^{22} cm^{-2}. Using a partial covering, we noted that the covering fraction parameter leaned to the higher boundary extreme, so that we could only measure a total absorption value of $(4 \pm 1) \times 10^{22}$ cm^{-2}; the electron temperature resulted poorly constrained and fixed, then, to 20 keV; the soft seed-photon temperature, the Γ parameter, and the unabsorbed 0.1–10 keV flux are 1.91 ± 0.35 keV, 1.94 ± 0.14, and $(5.8 \pm 1.7) \times 10^{-11}$ erg cm^{-2} s^{-1}, respectively. The multiplicative factor of the BAT model is 0.18 ± 0.07, which indicates that the XRT observation caught the source in brighter state with respect to long-term averaged flux. The unabsorbed flux measured during the XRT observation results a factor 2–3 higher than that observed in the simultaneous *NuSTAR* and *XMM–Newton* observations. We also found a similar amount of local absorption. In Fig. 3, we show data, best-fitting model, and residuals for the combined XRT and BAT broad-band spectrum.

Although we also obtained a satisfactorily description of the data with the `bwcycl` model, we do not go into detail, as slack constraints for many parameters prevented us to make meaningful comparisons or draw solid conclusions.

5 DISCUSSION

We exploited archival data based on *Swift*, XMM–*Newton*, and *Nu*STAR data available on IGR J18214-1318 for an updated study of the spectral and timing properties of this source. The BAT survey monitoring, spanning 13 yr, reveals a periodic modulation with $P_0 = 5.4246 \pm 0.0004$ d. The folded light curve shows a minimum

---

[6]We set this value according to the online N_H estimator at https://heasarc.gsfc.nasa.gov/cgi-bin/Tools/w3nh/w3nh.pl.
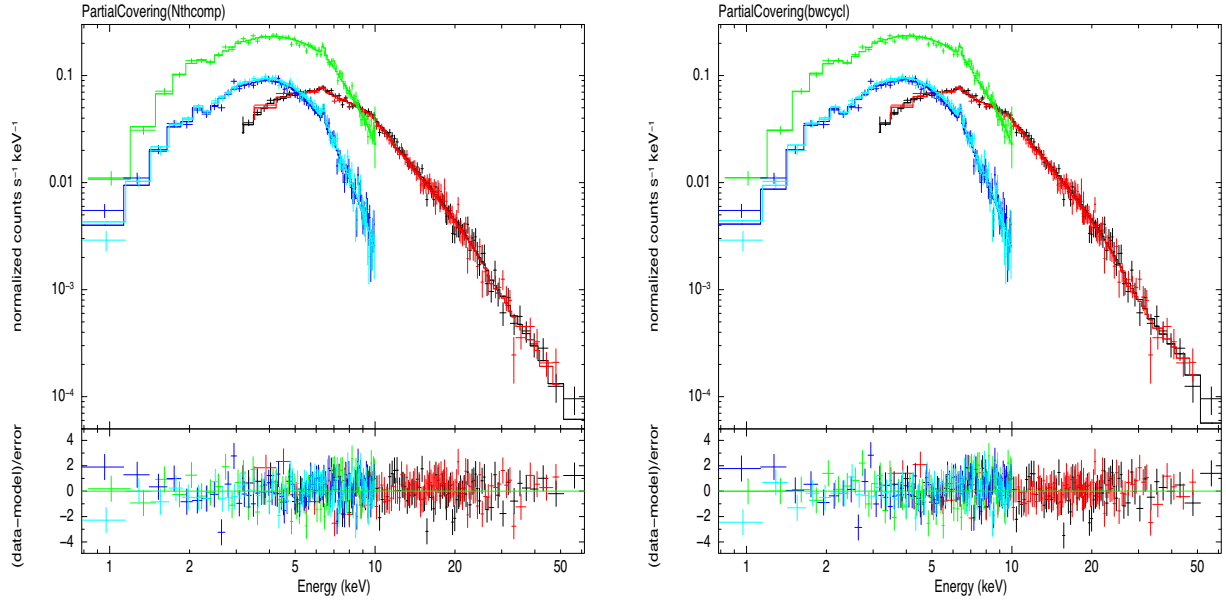
Figure 2. IGR J18214-1318 data and best-fitting models. NuSTAR/FPMA and NuSTAR/FPMB data in black and red colours; EPIC-PN data in red, EPIC/MOS1 and EPIC/MOS2 data in blue and cyan, respectively. Left-hand panel: data, best-fiting model, and residuals using the `tbabs*pcfabs*(nthcomp + gau)`. Right-hand panel: data, best-fitting model, and residuals using the `tabs*pcfabs*(bwcycl + gau)` model. Residuals in unit of standard deviations for the different data sets.
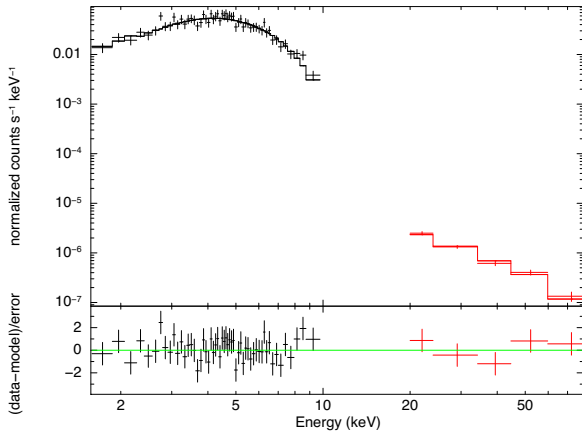

Figure 3. XRT and BAT broad-band spectrum of IGR J18214-1318. Top panel: data and best-fiting model `tbabs*pcfabs*(nthComp)`. Bottom panel: residuals in units of standard deviations.

consistent with none, or negligible, emission, thus suggesting the presence of an eclipse. We use Kepler's third law to derive the semimajor axis of the binary system assuming that P_0 is the system orbital period, $M_X = 1.4 M_\odot$ the mass of the NS, and $M_\star \simeq 30 M_\odot$ the companion's star mass (Martins, Schaerer & Hillier 2005):

$$a = (G P_0^2 (M_\star + M_X)/4\pi^2)^{1/3} \simeq 41 R_\odot. \qquad (1)$$

Considering that the radius of the companion star is $R_\star = {\sim}22 R_\odot$ (Martins et al. 2005), the semimajor axis length corresponds to ${\sim}2R_\star$. Such a tight orbital separation is common among wind-fed NSs accreting from an O-type companion star. With this geometry, assuming the orbit to be nearly edge-on, we expect the eclipse to last ${\sim}16$ per cent of the orbit. This is roughly consistent with the width of the eclipse observed in the folded light curve (Fig. 1 middle). The lack of detection in XRT observation 3, whose orbital phase
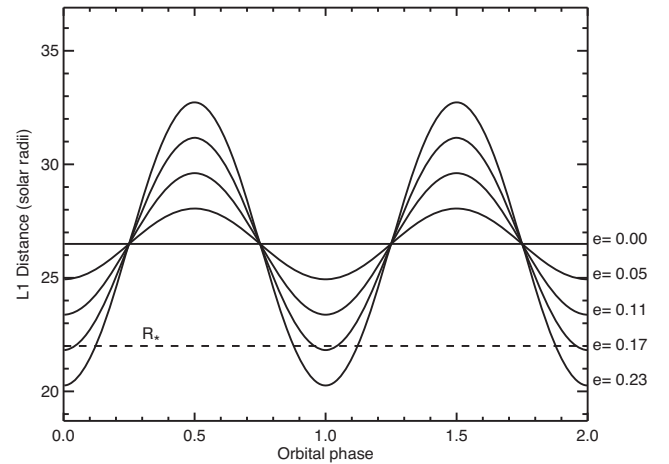

Figure 4. Distance of the L1 Lagrangian point from the companion star of IGR J18214-1318, as a function of the orbital phase, for different values of the orbital eccentricity. The dashed line represents the radius of the companion star.

falls marginally outside the dip, could be explained with enhanced absorption of the soft X-ray emission by the stellar wind, which results denser along the line of sight for smaller angular separation. However, we have also observed a significant flux variability in the soft X-rays, not related to the orbital phase, so we cannot exclude that this non-detection is due to a flux fluctuation because of a decrease of the accretion rate from the companion star. Knowing the radius of the supergiant companion, we can estimate the upper limit on the orbital eccentricity for a wind-fed accreting system. Fig. 4 shows how the Lagrangian point L1 varies with the orbital phase, for different eccentricities (Paczyński 1971). If the eccentricity were higher than ${\sim}0.17$, L1 would be within the companion star radius, and the accretion would be from Roche lobe overflow.

We have re-analysed the broad-band spectrum of IGR J18214-1318 extending the spectral analysis reported by Fornasini et al. (2017) using physical models to fit the data. A physical description is obtained either by a pure thermal Comptonization model or by a more complex model that takes into account also the bulk motion Comptonized component. In both cases, an excess below 2 keV in the residuals is indicative of an additional component. Fornasini et al. (2017) explained this excess either with a partial covering or with the addition of a hot thermal blackbody component, on the basis of an equivalent statistical result. Our fits are instead significantly better when using the partial covering rather than the blackbody. We found that the amount of local absorption can be uncertain by a factor of 2 depending on the choice of the continuum: the `bwcycl` model requires higher absorption values, similar to the results obtained by Fornasini et al. (2017), the `nthcomp` model requires half of this value and a higher covering fraction, close to 90 per cent, which suggests that local absorber embeds totally the compact object and reprocesses and re-emits the hard X-ray illuminating primary flux. The `bwcycl` model has been used under certain assumptions that the compact object is a magnetized NS with a bipolar field of 4×10^{12} G and the accretion rate is close to the critical luminosity (Becker & Wolff 2007). These assumptions should be proved with future observations. The luminosity depends quadratically on the distance and on the estimate for the local absorption, and our best guesses at the moment favour a luminosity of $\sim 10^{36}$ erg s^{-1}, which is expected below the critical luminosity. By adopting the appropriate transformations from our assumptions and from the best-fitting parameters, we derive the following physical quantities: the local mass accretion rate on the polar cap of the NS is of the order of 10^{10} g cm^{-2} s^{-1}, this builds a mound of material that has an altitude of ~ 1 m, a density of 13.5 g cm^{-2} and a thermal temperature of 8.2×10^8 K (section 6.3 in Becker & Wolff 2007). The very low inferred radius of the accretion column leads to a lower critical luminosity compared to the standard bright X-ray pulsars of the order of a few 10^{36} erg s^{-1}, which makes the adoption of this model reasonable (see a similar discussion for the applicability of this model in the case of another accreting X-ray pulsar D'Aì et al. 2017). Another important difference with other sources examined using this model is the derived δ value that sets the relative importance of the bulk versus thermal Comptonization ($\delta = 4$ y$_{\text{bulk}}$/y$_{\text{therm}}$, where the y-parameter describes the fractional energy increase in each of these processes Becker & Wolff 2007). For this source $\delta = 6$, which indicates that photons are mostly up-scattered by the free-fall electrons above the sonic point. Finally, we found that these models do also provide an adequate modelling to a *Swift* observation combined with an averaged long-term BAT spectrum, though the lower statistics did not allow a tight comparison of these different observations.

ACKNOWLEDGEMENTS

DATA AVAILABILITY

The data underlying this article are available in the HEASARC archive at https://heasarc.gsfc.nasa.gov/docs/archive.html and can be accessed with the following data set ID numbers: 30001140002 for *NuSTAR*, 0741470201 for *XMM–Newton*, 00035354001, 00035354003, 00035354005, and 00035354006 for Swift/XRT. Data for the Swift/BAT analysis are available in the HEASARC archive at https://heasarc.gsfc.nasa.gov/cgi-bin/W3Browse/swift.pl.

REFERENCES

Barthelmy S. D. et al., 2005, Space Sci. Rev., 120, 143
Becker P. A., Wolff M. T., 2005, ApJ, 630, 465
Becker P. A., Wolff M. T., 2007, ApJ, 654, 435
Bird A. J. et al., 2006, ApJ, 636, 765
Bird A. J. et al., 2016, ApJS, 223, 15
Bozzo E., Bernardini F., Ferrigno C., Falanga M., Romano P., Oskinova L., 2017, A&A, 608, A128
Burrows D. N. et al., 2004, Flanagan K. A., Siegmund O. H. W., Proc. SPIE Conf. Ser. Vol. 5165, X-Ray and Gamma-Ray Instrumentation for Astronomy XIII. SPIE, Bellingham, p. 201
Butler S. C. et al., 2009, ApJ, 698, 502
Coburn W., Heindl W. A., Rothschild R. E., Gruber D. E., Kreykenbohm I., Wilms J., Kretschmar P., Staubert R., 2002, ApJ, 580, 394
Corbet R. H. D., Krimm H. A., 2009, Astron. Telegram, 2008
Corbet R. H. D., Krimm H. A., 2010, Astron. Telegram, 3079
Corbet R. H. D., Krimm H. A., Barthelmy S. D., Baumgartner W. H., Markwardt C. B., Skinner G. K., Tueller J., 2010, Astron. Telegram, 2570
Corbet R. H. D., Barthelmy S. D., Baumgartner W. H., Krimm H. A., Markwardt C. B., Skinner G. K., Tueller J., 2010, Astron. Telegram, 2598
Corbet R. H. D., Barthelmy S. D., Baumgartner W. H., Krimm H. A., Markwardt C. B., Skinner G. K., Tueller J., 2010, Astron. Telegram, 2599
Corbet R. H. D., Krimm H. A., Skinner G. K., 2010, Astron. Telegram, 2559
Cusumano G., La Parola V., Romano P., Segreto A., Vercellone S., Chincarini G., 2010, MNRAS, 406, L16
Cusumano G., Segreto A., La Parola V., Masetti N., D'Aì A., Tagliaferri G., 2013, MNRAS, 436, L74
Cusumano G., Segreto A., La Parola V., D'Aì A., Masetti N., Tagliaferri G., 2013, ApJ, 775, L25
Cusumano G., Segreto A., La Parola V., Masetti N., D'Aì A., Tagliaferri G., 2015, MNRAS, 446, 1041
Cusumano G., La Parola V., Segreto A., D'Aì A., 2016, MNRAS, 456, 2717
D'Aì A., La Parola V., Cusumano G., Segreto A., Romano P., Vercellone S., Robba N. R., 2011, A&A, 529, A30
D'Aì A., Cusumano G., La Parola V., Segreto A., di Salvo T., Iaria R., Robba N. R., 2011, A&A, 532, A73
D'Aì A., Cusumano G., La Parola V., Segreto A., 2015, MNRAS, 451, 2835
D'Aì A., Cusumano G., Del Santo M., La Parola V., Segreto A., 2017, MNRAS, 470, 2457
Ferrigno C., Becker P. A., Segreto A., Mineo T., Santangelo A., 2009, A&A, 498, 825
Filliatre P., Chaty S., 2004, ApJ, 616, 469
Fornasini F. M., Tomsick J. A., Bachetti M., Krivonos R. A., Fürst F., Natalucci L., Pottschmidt K., Wilms J., 2017, ApJ, 841, 35
Gehrels N. et al., 2004, ApJ, 611, 1005
Harrison F. A. et al., 2013, ApJ, 770, 103
HI4PI Collaboration, 2016, A&A, 594, A116
Hill J. E. et al., 2004, in Flanagan K. A., Siegmund O. H. W., eds, Proc. SPIE Conf. Ser. Vol. 5165, X-Ray and Gamma-Ray Instrumentation for Astronomy XIII. SPIE, Bellingham, p. 217
in 't Zand J. J. M., 2005, A&A, 441, L1
Jansen F. et al., 2001, A&A, 365, L1
Kaastra J. S., Bleeker J. A. M., 2016, A&A, 587, A151
Krimm H. A. et al., 2013, ApJS, 209, 14
Krivonos R., Tsygankov S., Lutovinov A., Revnivtsev M., Churazov E., Sunyaev R., 2012, A&A, 545, A27

La Parola V., Cusumano G., Romano P., Segreto A., Vercellone S., Chincarini G., 2010, MNRAS, 405, L66

La Parola V., Cusumano G., Segreto A., D'Aì A., Masetti N., D'Elia V., 2013, ApJ, 775, L24

La Parola V., Segreto A., Cusumano G., Masetti N., D'Aì A., Melandri A., 2014, MNRAS, 445, L119

Lebrun F. et al., 2003, A&A, 411, L141

Martinez-Nunez S. et al., 2017, Space Sci. Rev., 212, 59

Martins F., Schaerer D., Hillier D. J., 2005, A&A, 436, 1049

Masetti N. et al., 2006, A&A, 459, 21

Negueruela I., Smith D. M., Reig P., Chaty S., Torrejón J. M., 2006, in Wilson A., ed., The X-ray Universe 2005, Vol. 604. ESA Publications Division, Noordwijk, The Netherlands, p. 165

Negueruela I., Smith D. M., Harrison T. E., Torrejón J. M., 2006, ApJ, 638, 982

Paczyński B., 1971, ARA&A, 9, 183

Reig P., Negueruela I., Papamastorakis G., Manousakis A., Kougentakis T., 2005, A&A, 440, 637

Rodriguez J., Tomsick J. A., Chaty S., 2009, A&A, 494, 417

Segreto A., Cusumano G., Ferrigno C., La Parola V., Mangano V., Mineo T., Romano P., 2010, A&A, 510, A47

Segreto A., Cusumano G., La Parola V., D'Aì A., Masetti N., D'Avanzo P., 2013, A&A, 557, A113

Segreto A., La Parola V., Cusumano G., D'Aì A., Masetti N., Campana S., 2013, A&A, 558, A99

Sguera V. et al., 2005, A&A, 444, 221

Standish E. M., Jr, 1982, A&A, 114, 297

Tomsick J. A., Chaty S., Rodriguez J., Walter R., Kaaret P., 2008, ApJ, 685, 1143

Ubertini P. et al., 2003, A&A, 411, L131

Verner D. A., Ferland G. J., Korista K. T., Yakovlev D. G., 1996, ApJ, 465, 487

Wilms J., Allen A., McCray R., 2000, ApJ, 542, 914

Winkler C. et al., 2003, A&A, 411, L1

Zdziarski A. A., Johnson W. N., Magdziarz P., 1996, MNRAS, 283, 193

Zurita Heras J. A., Chaty S., 2008, A&A, 489, 657

Zycki P. T., Done C., Smith D. A., 1999, MNRAS, 309, 561

This paper has been typeset from a TEX/LATEX file prepared by the author.